Supplemental Materials

Molecular Biology of the Cell

Ren et al.

SUPPLEMENTAL MATERIALS

A Phosphatidylinositol Transfer Protein Integrates Phosphoinositide Signaling With Lipid Droplet Metabolism To Regulate a Developmental Program of Nutrient Stress-Induced Membrane Biogenesis

Jihui Ren[1,2†], Coney Pei-Chen Lin[3], Manish C. Pathak[4], Brenda R.S. Temple[5], Aaron H. Nile[2], Carl J. Mousley[2], Mara C. Duncan[6], Debra M. Eckert[7], Thomas J. Leiker[8], Pavlina T. Ivanova[9], David S. Myers[9], Robert C. Murphy[8], H. Alex Brown[9], Jolien Verdaasdonk[6], Kerry S. Bloom[6], Eric A. Ortlund[4], Aaron M. Neiman[3], and Vytas A. Bankaitis[2†]

[1]Lineberger Comprehensive Cancer Center, School of Medicine
University of North Carolina at Chapel Hill
Chapel Hill, North Carolina 27599-7090 USA

[2]Department of Molecular and Cellular Medicine
Department of Biochemistry and Biophysics
Department of Chemistry
Texas A&M University
College Station, Texas 77843-1114 USA

[3]Department of Biochemistry and Cell Biology
Stony Brook University
Stony Brook, NY 11794-5215 USA

[4]Department of Biochemistry
Emory University School of Medicine
Atlanta, GA 30322 USA

[5]R. L. Juliano Structural Bioinformatics Core
University of North Carolina at Chapel Hill,
Chapel Hill, North Carolina 27599-7260 USA

[6]Department of Biology
University of North Carolina at Chapel Hill,
Chapel Hill, North Carolina 27510 USA

[7]Department of Biochemistry
University of Utah School of Medicine
Salt Lake City, UT 84112-5650 USA

[8]Department of Pharmacology
University of Colorado Health Sciences Center
Denver, CO 80045-0511 USA

[9]Department of Pharmacology
Vanderbilt University School of Medicine
Nashville, TN 37232-6600 USA

SUPPLEMENTAL TEXT

Novel features of the Sfh3 fold. While the core fold is conserved between Sec14 and Sfh3, there are significant conformational differences between the Sec14 and Sfh3 'open' structures. One major distinction between the Sec14/Sfh1- and Sfh3-fold involves the string motif. This substructure lies behind the β-sheet floor of the lipid-binding pocket of Sec14-like proteins and, for Sfh3, is extended relative to Sec14/Sfh1 by an extra β-strand (B_6) and two helices (Suppl. Fig. S2A). Another notable Sfh3 feature is that interpretable electron density for the N-terminal half of helix A_7 ($_{210}$VPGNSKIP$_{217}$) was missing from the electron density map (Suppl. Fig. S2B). In apo-Sec14 and holo-Sfh1 structures, the corresponding motif is well-ordered and produces a pronounced bend in the cognate helix (Sha *et al.*, 1998; Schaaf *et al.*, 2008). The presumed conformational flexibility of the Sfh3 $_{210}$VPGNSKIP$_{217}$ motif renders the lipid-binding pocket wider and shallower than those of the PtdIns/PtdCho-binding proteins Sec14 and Sfh1 (Suppl. Fig. S2B). Finally, the electrostatic charge distribution across the Sfh3 lipid binding pocket exhibited a polarity reverse to that of the Sec14 and Sfh1 lipid binding pockets (Suppl. Fig. S2C). These data indicate the Sfh3 lipid binding pocket defines a significantly different chemical environment than the corresponding environments of the classical Sec14 and Sfh1 PITPs.

Signature features of the Sfh3 lipid-binding pocket. To further probe the functional properties of the Sfh3 lipid binding pocket, we aligned the primary sequences of 66 fungal Sfh3 orthologs. The analysis identified 104 residues that are uniquely conserved amongst Sfh3-like proteins. Of these, 90 frame a region of the hydrophobic pocket that corresponds to the lipid-binding sub-structures of other Sec14-like proteins. The residues conserved among Sec14 orthologs, and those conserved among Sfh3-like proteins, are highlighted in magenta in Suppl. Figs. S3A and S3B, respectively. In

both sets, the 'signature' residues distribute predominantly throughout the corresponding lipid-binding pockets – forecasting that members of each Sec14-like PITP subfamily likely bind similar lipid ligands within the subfamily. For the Sec14 subfamily, two ligands are PtdIns and PtdCho. Superposition of the respective binding poses into the Sec14 and Sfh3 structures shows the phospholipids nestle within the corresponding conserved regions (Suppl. Figs. S3A,3B).

The similarities and the distinctions of the pocket chemistries of Sfh3 orthologs, relative to those of Sec14/Sfh1 orthologs, are reflected in the corresponding primary sequence signatures. The residues within the lipid-binding region of the hydrophobic pocket unique to Sfh3 orthologs (i.e. diverged from Sec14 orthologs) are colored orange in Suppl. Fig. S3C. Residues conserved between the Sec14- and Sfh3-subfamilies are rendered magenta. When residues shared between Sec14- and Sfh3-like proteins are distinguished from residues unique to Sfh3-like proteins, the conservation of the PtdIns-binding barcode in both Sfh3 and Sec14 orthologs becomes readily apparent (Suppl. Fig. S3C, left panel). This shared structural property is congruent with the common PtdIns-binding/transfer activities of both subfamilies of Sec14-like proteins.

Divergences of the Sfh3 pocket signature from that of Sec14 are striking in the region of the PtdCho-headgroup binding motif (Suppl. Fig. S3C, right panel). The Sec14/Sfh1 PtdCho-binding barcode consists of two primary components. Sec14 residues S_{175} and T_{177} coordinate the PtdCho headgroup phosphate deep within the hydrophobic pocket interior, while residues Y_{124} and Y_{153} stabilize the buried choline moiety via cation-π interactions (Schaaf *et al.*, 2008). The Sfh3 residues which correspond to Sec14 residues S_{175} and T_{177} are L_{195} and L_{197} (Suppl. Fig. S3D), and the bulky Leu side-chains are incompatible with PtdCho binding by the Sec14/Sfh1 on steric grounds (Schaaf *et al.*, 2008; Schaaf *et al.*, 2011). Sfh3 L_{158} and L_{181} correspond to Sec14 Y_{124} and Y_{153} (Suppl. Fig. S3D). These Sfh3 Leu side-chains cannot engage in cation-π interactions with the choline

headgroup. Consistent with these divergent structural features, no PtdCho transfer activity was detected for Sfh3 (Suppl. Fig. S3E). The conservation of these signature Leu residues among Sfh3 orthologous suggests an important functional role for these residues. To determine whether these divergent residues are required for Sfh3 biological activity, each was converted to the corresponding Sec14 residue. Whereas Sfh3^{L195S}, Sfh3^{L197T} and Sfh3^{L158Y} retained in vivo function, sfh3^{L181Y} was a loss-of-function mutant that accumulated to steady-state levels in cells that were comparable to those measured for Sfh3.

SUPPLEMENTAL METHODS

Neutral lipidomics. LDs were purified and frozen in liquid nitrogen before lipid extraction and analysis. Weighed aliquots of frozen LDs (kept at -70°C) were thawed, and the internal standards [$^{13}C_{18}$]-cholesteryl ester (1) and 14:0/16:1/14:0-D_5 labeled triacylglycerol (Avanti Polar Lipids, Alabaster, AB) (500 ng, and 50 ng, respectively) were added after addition of 2 ml PBS. Each sample was extracted twice with 2 mL of 25% ethyl acetate/isooctane. The samples were then centrifuged at 3,000 RPM for 3 min. The organic (upper) layers combined in a previously solvent rinsed culture tube. The solvent was removed under a gentle stream of nitrogen and the extract reconstituted in dichloromethane with 4% v/v methyl *t*-butyl ether (MTBE)/isooctane (800 μl). Chromatographic separations were carried out using a normal phase Phenomenex Luna 5 μm particle size, 150 mm x 2 mm id silica column. Total flow into the mass spectrometer (AB Sciex 4000 QTRAP linear ion trap quadrupole mass spectrometer, Thornhill, Ontario, Canada) is 0.2mL/min. A linear normal phase solvent gradient system was generated using 100% isooctane (mobile phase A) and mobile phase B, MTBE/isooctane (1/1) from 8% mobile phase B for the first 7 min, then raised to 30% from 7 min to 25 min, then raised from 30% to 90% from 25 min to 29min and held at 90% mobile phase B for 2 min. The column was then re-equilibrated back to 8% mobile phase B. For separations 1 μL samples were injected onto the column using an autosampler.

Neutral lipids were analyzed, as ammonium adduct ions, using electrospray ionization conditions in positive ion mode. A 10 mM ammonium acetate (95% acetonitrile/5% water) solution was introduced post-column just prior to the electrospray interface at a flow-rate of 0.030 mL/min as previously described (Hutchins *et al.*, 2008). For quantitative analysis of the ergosteryl esters, specific MRM experiments for each molecular species were carried out during the first 5 min of the

HPLC separation, and the ratio of the abundance of the MRM transition converted to nmoles using the signal of the internal standard and a previously determined standard curve (Hutchins *et al.*, 2008). A separate aliquot was used to determine the specific ergosteryl esters present in the LD extract using the ion trap function to detect $[M+NH_4]^+$ followed by collisional activation. Each ergosteryl ester yielded a common product ion as the most abundant product ion at m/z 379.3. The TAG molecular species were quantitated from the abundance of the $[M+NH_4]^+$ recorded in full mass scanning mode from m/z 700-1000 after the first 5 min of the HPLC separation, as previously described (Hutchins *et al.*, 2008).

Phospholipidomics. LDs were purified and frozen in liquid nitrogen before lipid extraction and analysis. Glycerophospholipids from yeast LDs were extracted using a modified Bligh and Dyer procedure (Bligh and Dyer, 1959). LDs isolated from an equivalent of 10^9 cells were homogenized in 800 µl of ice-cold 0.1N HCl:CH_3OH (1:1) by vortexing for about 1 min on ice with addition of 100µl acid-washed glass beads (0.5 mm glass beads, Biospec Products, Inc. Bartlesville, OK). Suspension was then transferred to cold 1.5 ml Eppendorf tubes and mixed with 400µl of cold $CHCl_3$ for 1 min. The extraction proceeded with centrifugation (5 min, 4°C, 18,000 x g) to separate the two phases. Lower organic layer was collected, and solvent evaporated under a stream of N_2 gas. The resulting lipid film was dissolved in 100µl of isopropanol:hexane:100mM NH_4COOH(aq) 58:40:2 (mobile phase A). Quantification of glycerophospholipids was achieved using an LC-MS technique employing synthetic (non-naturally occurring) diacyl and lysophospholipid standards. Typically, 200ng of each odd-carbon standard was added to each sample. Glycerophospholipids were analyzed on an Applied Biosystems/MDS SCIEX 4000 Q TRAP hybrid triple quadrupole/linear ion trap mass spectrometer (Applied Biosystems, Foster City, CA, USA) and a

Shimadzu high pressure liquid chromatography system with a Phenomenex Luna Silica column (2 × 250 mm, 5-μm particle size) using a gradient elution as previously described (Ivanova *et al.*, 2007; Myers *et al.*, 2011). The identification of the individual species by LC/MS/MS was based on their chromatographic and mass spectral characteristic. These analyses allowed identification of the fatty acid moieties but did not determine their position on the glycerol backbone (*sn-1* versus *sn-2*).

Phospholipase D activity measurements. PLD activities were measured by assaying release of free choline into growth medium using a coupled choline oxidase assay as described (Xie *et al.*, 2001). Yeast were cultured at 26°C in minimal defined choline-free Wickerham's medium supplemented with inositol (100μM). Cells were pelleted, washed with water, and resuspended in fresh choline-free medium at 37°C. After three hours, cells were pelleted, the culture supernatants collected, and supernatants passed through a 0.45-micron pore-size filter. Choline contents of supernatant samples were determined by a coupled reaction where the H_2O_2 formed as product of choline oxidation by choline oxidase was reacted with aminoantipyrine and phenol to form quinoneimine (Warnick, 1986). Quinoneimine was quantified spectrophotometrically at 490 nm, and choline standards were used in converting A_{490} measurements to absolute choline concentrations.

SUPPLEMENTAL REFERENCES

Hutchins PM, Barkley RM, and Murphy RC (2008) Separation of cellular nonpolar neutral lipids by normal-phase chromatography and analysis by electrospray ionization mass spectrometry. *J Lipid Res* ***49***: 804-813.

Ivanova PT, Milne SB, Byrne MO, Xiang Y, and Brown HA (2007) Glycerophospholipid identification and quantitation by electrospray ionization mass spectrometry. *Methods in enzymology* ***432***: 21-57.

Myers DS, Ivanova PT, Milne SB, and Brown HA (2011) Quantitative analysis of glycerophospholipids by LC-MS: acquisition, data handling, and interpretation. *Biochim Biophys Acta* ***1811***: 748-757.

Schaaf G, Dynowski M, Mousley CJ, Shah SD, Yuan P, Winklbauer EM, de Campos MK, Trettin K, Quinones MC, Smirnova TI, Yanagisawa LL, Ortlund EA, and Bankaitis VA (2011) Resurrection of a functional phosphatidylinositol transfer protein from a pseudo-Sec14 scaffold by directed evolution. *Mol Biol Cell* ***22***: 892-905.

Schaaf G, Ortlund EA, Tyeryar KR, Mousley CJ, Ile KE, Garrett TA, Ren J, Woolls MJ, Raetz CR, Redinbo MR, and Bankaitis VA (2008) Functional anatomy of phospholipid binding and regulation of phosphoinositide homeostasis by proteins of the sec14 superfamily. *Mol Cell* ***29***: 191-206.
Sha B, Phillips SE, Bankaitis VA, and Luo M (1998) Crystal structure of the Saccharomyces cerevisiae phosphatidylinositol-transfer protein. *Nature* ***391***: 506-510.

Warnick GR (1986) Enzymatic methods for quantification of lipoprotein lipids. *Methods in enzymology* ***129***: 101-123.

Xie Z, Fang M, and Bankaitis VA (2001) Evidence for an intrinsic toxicity of phosphatidylcholine to Sec14p-dependent protein transport from the yeast Golgi complex. *Mol Biol Cell* ***12***: 1117-1129.

LEGENDS TO SUPPLEMENTAL FIGURES

Supplemental Figure S1. (A) Recombinant Sfh3 and sfh3^{T264W} purify as dimers. Analytical equilibrium sedimentation analyses of Sfh3. Experiments were performed at 4ºC in 50mM sodium phosphate (pH 7.5), 300mM NaCl, 0.5 mM TCEP (Tris(2-carboxyethyl)phosphine-HCl) buffer at two rotor speeds (9,000 and 12,000RPM). Three concentrations of Sfh3 were analyzed (8μM, 4μM, 2μM). All data were globally fit to a single ideal species with a floating molecular weight using the non-linear least squares algorithms in the Hetero analysis software (Cole, 2004). The 9,000 RPM data are shown with the global fit. Residual differences between data and fit are shown at bottom. Estimated molecular mass for Sfh3 was 80.103 kDa (MW_{obs}/MW_{calc} = 1.97). **(B, C)** Gel-filtration chromatograms of purified recombinant Sfh3 **(B)** and sfh3^{T264W} **(C)** are shown. Both Sfh3 and sfh3^{T264W} eluted at an elution volume (Ve) that corresponded to an apparent M_r = 80 kDa. Also shown are elution traces of bovine serum albumin (BSA, 67 kDa) and aldolase (158 kDa). **(D,E)** Circular dichroism analysis of purified recombinant Sfh3 **(D)** and sfh3^{T264W} **(E)**. The CD signature indicates sfh3^{T264W} is well-folded and exhibits a trace very similar to that exhibited by Sfh3. The deeper absorbance trough at 201-203nM for sfh3^{T264W} (relative to Sfh3) was the result of incorporating an additional Trp residue into the mutant derivative ($T_{264}W$ missense substitution).

Supplemental Figure S2. Sfh3 manifests distinctive structural features compared with Sec14 and Sfh1. **(A)** Cartoon representation of Sfh3 (gray) highlighting novel structural elements unique to Sfh3 in red (PDB ID 4M8Z). Yellow β-strands form the lipid binding pocket floor. **(B)** Disordered loop ($_{210}$VPGNSKIP$_{217}$) in Sfh3 is indicated by red circle and contributes to a larger and shallower lipid binding pocket. **(C)** Electrostatic surfaces for the lipid binding pockets of Sec14 (1AUA) and

Sfh3 calculated using the Adaptive Poisson-Boltzmann Solver within PyMOL (Schrödinger, LLC). Protein backbone is depicted in white transparent cartoon. Electrostatic potentials are mapped to the solved accessible surfaces with positive values in blue and negative values in red (range: -3kT to 3kT). Gating helices for Sec14 and Sfh3 are highlighted by arrowed bars.

Supplemental Figure S3. Homology comparisons of Sec14 **(A)** or Sfh3 **(B)** with their corresponding fungal orthologs. The conserved residues within each ortholog family (magenta) were mapped onto their respective surface structures (Sec14, sand; Sfh3, cyan). PtdIns and PtdCho were modeled into each structure (PtdIns, blue; PtdCho, white). **(C)** Conserved residues within Sfh3 ortholog family were divided into two groups. Magenta residues highlight conserved residues within the Sfh3 ortholog family that are also conserved with Sec14 orthologs (left panel). Orange rendering highlights residues conserved within the Sfh3 ortholog family that diverge from their cognates in Sec14 orthologs (right panel). **(D)** The PtdCho (magenta) binding pocket in Sec14/Sfh1 (cyan) is superposed onto the corresponding residues in Sfh3 (green). Residues within 4.2 Å of the PtdCho head group are depicted in stick representation. Note that Sfh3 lacks the aromatic cage which supports PtdCho binding by Sec14 and Sfh1. Images were generated in PyMOL (Schrödinger, LLC). Residues L_{158} (#), L_{181} (+) and L_{195} (*) are conserved among Sfh3 orthologs and are incompatible with PtdCho binding. **(E)** Purified recombinant Sec14, Sfh3 and sfh3^{T264W} were assayed for PtCho-transfer activity in a 0.004, 0.2, 1, 5, and 25μg step series of protein. Average values and standard deviation are given (n=4).

Supplemental Figure S4. Sfh3OE does not inhibit PLD activity. **(A)** Equivalent numbers of isogenic yeast cells with the indicated genotypes were spotted in 3-fold dilution series (left to right,

as indicated) onto SD agar and incubated at the permissive- and restrictive temperatures of 30ºC and 37ºC, respectively. Images were taken after 48hr incubations. Sfh3OE phenocopies *spo14*Δ (PLD structural gene deletion allele) in compromising 'bypass Sec14' by *kes1*Δ and *cki1*Δ as evidenced by lack of growth at 37ºC for *sec14*^{ts} mutants carrying either allele in a *spo14*Δ or Sfh3OE genetic background. **(B)** Qualitative bioassay for PLD-dependent choline excretion. A yeast choline auxotroph was plated onto choline-free agar as an indicator lawn, and equivalent cell numbers of the indicated mutants were spotted onto the lawn. Image was collected after 48hr incubation at 30ºC. Halo size reports extent of choline excretion and subsequent cross-feeding of the choline auxotroph indicator strain. WT cells do not express PLD activity, *spo14*Δ mutants cannot generate free choline, and *sec14*^{ts} mutants exhibit constitutively elevated PLD activity. The *cki1* allele prevents choline salvage into PtdCho biosynthesis and therefore allows a genuine assessment of free choline production. Sfh3OE does not diminish PLD-mediated choline release. **(C)** Quantitative assay for PLD-dependent choline excretion. The experiment outlined in (B) was repeated in a format where the liquid media in which the strains of indicated genotype were grown were measured for free choline content by chemical assay.

Supplemental Figure S5. Overexpression of Sfh3 uniquely evokes LD accumulation. **(A)** WT yeast were transformed with episomal plasmids driving high-level expression of the indicated Sec14-like PITP structural genes. Cells were cultured in minimal media to stationary phase, LDs were stained with BODIPY493/503, and collected fluorescence images superposed onto the corresponding DIC images. Sfh3OE cells exhibited an average load of 15 ± 3 LDs/cell vs. 8 ± 2 LDs/cell for WT controls and cells overexpressing any one of the other Sec14-like proteins. Bar, 2μm. **(B)** Ultrastructures of WT, *sfh3*Δ and Sfh3OE cells. Yeast were cultured in minimum SD

medium to stationary phase before processing and examination of cell morphologies by conventional TEM. The electron-transparent structures are LDs. Nucleus (N); bar, 0.5μm.

Supplemental Figure S6. Lipidomic profiling of purified LDs. Quantitative profiling of **(A)** phospholipids (WT, white bars; *sfh3Δ*, gray bars; Sfh3OE, black bars) (key: PtdOH, phosphatidic acid; PtdCho, phosphatidylcholine; PtdEth, phosphatidylethanolamine; PtdGro, phosphatidylglycerol; PtdIns, phosphatidylinositol; PtdSer, phosphatidylserine), **(B)** ergosteryl esters, and **(C)** triacylglycerols in LDs purified from yeast of the indicated genotypes. Shown are the average molar percentages of the major lipid species. The lipid species are listed in rank order of abundance in (B) and (C).

LEGENDS TO SUPPLEMENTAL TABLES

Supplemental Table S1. Sporulation efficiencies as a function of Sfh3 levels.

Supplemental Table S2. Sporulation efficiency vs. meiotic division efficiency.

Supplemental Table S3. The phospholipid compositions are shown for LDs purified from WT, Sfh3OE, and *sfh3*Δ strains as indicated (n=3 per strain), and are expressed as mol% for each phospholipid species (PA, phosphatidic acid; PC, phosphatidylcholine; PE, phosphatidylethanolamine; PG,phosphatidylglycerol; PI, phosphatidylinositol; PS, phosphatidylserine).

Supplemental Table S4. The mol% for each ergosteryl ester molecular species is provided for LDs purified from WT, *sfh3*Δ and Sfh3OE strains, as indicated.

Supplemental Table S5. The mol% for each TAG molecular species is provided for LDs purified from WT, *sfh3*Δ and Sfh3OE strains, as indicated.

Supplemental Table S1. Sporulation efficiencies as a function of Sfh3 levels.

Strain name	*SFH3* locus genotype	Sporulation efficiency (%)
WT	*SFH3 X SFH3*	42.1±1.6
sfh3Δ	*sfh3Δ::KanMx X sfh3Δ::KanMx*	46.1±2.0
Sfh3OE$^{1/2}$	*SFH3 X PMA1^{pro}-Sfh3-ADH^{ter}::Ura3*	18.2±1.9
Sfh3OE	*PMA1^{pro}-Sfh3-ADH^{ter}::Ura3 X PMA1^{pro}-Sfh3-ADH^{ter}::Ura3*	5.5±0.3
sfh3^{T264W}OE	*PMA1^{pro}-sfh3^{T264W}-ADH^{ter}::Ura3 X PMA1^{pro}-sfh3^{T264W}-ADH^{ter}::Ura3*	42.1±1.8

The diploid is generated by crossing BY4741 with BY4742. Sporulation efficiencies were assessed after 5 days in sporulation medium as described by Neiman (1998). Minimally, 600 cells were counted for each strain over three independent experiments. The final sporulation efficiencies counted asci with 2, 3 or 4 mature spores.

Supplemental Table S2. Meiotic division efficiency vs sporulation efficiency.

	24 hours		48 hours	
	Sporulation (%)	Meiosis II (%)	Sporulation (%)	Meiosis II (%)
wt	7.0±1.0	10.7±1.2	14.0±1.8	21.2±2.8
sfh3Δ	11.1±1.2	10.8±0.8	21.4±1.8	22.4±1.4
Sfh3OE	0.9±0.2	4.9±0.8	2.0±0.4	7.5±1.8

The diploid is generated by crossing BY4741 with BY4742. Both sporulation efficiencies and percentages of cells undergoing meiosis II were assessed after 24 and 48 hours in sporulation medium as described by Neiman (1998). Minimally, 600 cells were counted for each strain over three independent experiments. The final sporulation efficiencies counted asci with 2, 3 or 4 mature spores.

Supplemental Table S3. Phospholipid composition of purified LDs.

phospholipid species	Wt (% ±STD)	Sfh3OE (% ±STD)	*sfh3Δ* (% ±STD)
PA(32:2)	0.4±0.0	0.7±0.2	0.3±0.1
PA(32:1)	1.7±0.9	1.7±0.4	1.0±0.4
PA(34:2)	0.6±0.4	0.6±0.2	0.3±0.1
PA(34:1)	0.6±0.4	0.4±0.2	0.1±0.1
PA(36:1)	0.3±0.2	0.3±0.1	0.2±0.0
PC(26:1)	0.3±0.2	0.2±0.0	0.1±0.0
PC(26:0)	0.3±0.2	0.3±0.0	0.2±0.1
PC(28:1)	0.5±0.3	0.5±0.1	0.3±0.0
PC(28:0)	0.8±0.1	0.8±0.1	1.1±0.0
PC(30:2)	0.3±0.4	0.2±0.0	0.1±0.0
PC(30:1)	0.8±0.4	0.6±0.0	0.5±0.0
PC(31:0)	0.8±0.4	0.7±0.1	0.4±0.1
PC(32:2)	4.1±1.0	4.6±0.2	3.1±0.2
PC(32:1)	7.3±1.8	7.7±0.9	8.8±0.8
PC(32:0)	1.4±0.0	1.2±0.1	2.0±0.3
PC(34:3)	0.2±0.2	0.4±0.1	0.3±0.0
PC(34:2)	2.5±0.5	2.4±0.1	1.7±0.2
PC(34:1)	3.8±0.6	3.4±0.4	4.4±0.4
PC(34:0)	1.5±0.5	1.4±0.2	2.5±0.4
PC(36:2)	1.6±0.5	1.2±0.1	1.0±0.1
PC(36:1)	2.7±0.6	2.2±0.2	4.3±0.6
PC(36:0)	0.5±0.1	0.5±0.0	1.1±0.3
PC(38:2)	0.7±0.7	0.4±0.2	0.2±0.1
PC(38:1)	2.3±0.8	3.3±0.4	2.4±0.9
PC(42:1)	5.7±1.5	6.2±0.8	7.5±0.5
PC(43:1)	2.7±0.4	2.7±0.2	3.5±0.2
PC(44:1)	1.2±0.4	1.1±0.2	2.4±0.4
PC(46:1)	0.5±0.1	0.7±0.3	0.4±0.1
PE(32:2)	3.1±0.8	4.5±0.3	2.4±0.3
PE(32:1)	5.9±1.7	6.6±0.9	5.7±1.2
PE(33:1)	0.2±0.1	0.2±0.0	0.1±0.0
PE(34:2)	3.8±0.7	4.6±0.2	3.5±0.4
PE(34:1)	8.5±1.4	7.8±1.6	9.7±3.0
PE(34:0)	1.0±0.4	0.9±0.3	1.9±0.9
PE(36:2)	1.0±0.2	1.0±0.1	1.3±0.2
PE(36:1)	0.6±0.1	0.6±0.1	0.7±0.3
PE(41:1)	0.4±0.1	0.3±0.1	0.3±0.1
PE(42:1)	0.2±0.1	0.2±0.0	0.2±0.0
PE(44:1)	0.3±0.1	0.2±0.0	0.2±0.1
PG(32:1)	0.2±0.1	0.2±0.0	0.1±0.0
PG(34:1)	0.3±0.1	0.2±0.1	0.2±0.1
PG(36:2)	0.2±0.1	0.2±0.0	0.1±0.0
PI(26:0)	0.1±0.0	0.3±0.1	0.1±0.0

PI(28:1)	0.1±0.0	0.1±0.0	0.0±0.0
PI(28:0)	0.4±0.1	0.6±0.1	0.3±0.1
PI(30:1)	0.1±0.0	0.2±0.0	0.1±0.0
PI(30:0)	0.3±0.0	0.4±0.1	0.2±0.1
PI(32:2)	0.2±0.1	0.2±0.1	0.1±0.0
PI(32:1)	1.8±0.4	2.3±0.4	1.3±0.6
PI(32:0)	0.4±0.1	0.4±0.1	0.3±0.2
PI(33:1)	0.1±0.0	0.1±0.0	0.0±0.0
PI(34:2)	0.2±0.1	0.2±0.1	0.1±0.0
PI(34:1)	2.8±0.7	2.9±0.3	1.9±0.8
PI(34:0)	0.5±0.1	0.5±0.1	0.4±0.2
PI(35:1)	0.0±0.0	0.1±0.0	0.0±0.0
PI(36:2)	0.1±0.0	0.1±0.0	0.0±0.0
PI(36:1)	0.7±0.2	0.9±0.1	0.6±0.3
PI(36:0)	0.1±0.0	0.1±0.0	0.1±0.1
PI(38:1)	0.1±0.0	0.1±0.0	0.1±0.0
PI(42:1)	0.0±0.0	0.0±0.0	0.0±0.0
PI(43:1)	0.0±0.0	0.0±0.0	0.0±0.0
PI(44:1)	0.0±0.0	0.0±0.0	0.0±0.0
PS(32:2)	0.9±0.2	0.8±0.1	0.6±0.2
PS(32:1)	3.5±0.4	3.4±0.4	3.6±1.5
PS(34:2)	1.8±0.2	1.4±0.3	1.8±0.7
PS(34:1)	11.0±1.1	9.4±0.8	9.7±2.4
PS(34:0)	0.7±0.2	0.5±0.1	0.7±0.2
PS(36:4)	0.9±0.1	0.8±0.1	0.8±0.2
PS(36:1)	1.1±1.0	0.7±0.1	0.3±0.0

Phospholipids were extracted from purified LDs, subjected to mass spectrometry, and identified. Phospholipid molecular species and corresponding mol percentages for each are listed.

Supplemental Table S4. Ergosteryl ester composition of purified LDs.

Ergosteryl Ester species	WT (% ± STD)	Sfh3OE (% ± STD)	*sfh3Δ* (% ± STD)
16:1	48.5±7.3	52.5±3.3	49.9±3.4
18:1	33.4±3.2	27.2±2.2	29.5±0.7
18:0	10.1±5.1	9.5±2.4	11.3±2.4
16:0	6.8±1.8	9.4±1.7	8.9±1.0
20:0	0.5±0.4	0.5±0.1	0.4±0.2
14:1	0.2±0.2	0.4±0.3	0.3±0.0
17:1	0.1±0.1	0.1±0.1	0.1±0.0
20:1	0.1±0.1	0.1±0.0	0.1±0.1
16:2	0.1±0.0	0.1±0.1	0.1±0.0
18:2	0.1±0.0	0.1±0.1	0.0±0.0
17:0	0.1±0.1	0.1±0.1	0.0±0.0
14:0	0.0±0.0	0.0±0.0	0.0±0.0
15:0	0.0±0.0	0.0±0.0	0.0±0.0
15:1	0.0±0.0	0.0±0.0	0.0±0.0
18:3	0.0±0.0	0.0±0.0	0.0±0.0
20:2	0.0±0.0	0.0±0.0	0.0±0.0
20:3	0.0±0.0	0.0±0.0	0.0±0.0
20:4	0.0±0.0	0.0±0.0	0.0±0.0
22:0	0.0±0.0	0.0±0.0	0.0±0.0
22:1	0.0±0.0	0.0±0.0	0.0±0.0
22:2	0.0±0.0	0.0±0.0	0.0±0.0
22:4	0.0±0.0	0.0±0.0	0.0±0.0
22:5	0.0±0.0	0.0±0.0	0.0±0.0
22:6	0.0±0.0	0.0±0.0	0.0±0.0

Ergosteryl esters were extracted from purified LDs, subjected to mass spectrometry, and identified. Ergosteryl ester molecular species and corresponding mol percentages for each are listed.

Supplemental Table S5. Triglyceride composition of purified LDs.

TAG species	WT (% ± STD)	Sfh3OE (% ± STD)	*sfh3Δ* (% ± STD)
50:3	10.43±0.26	9.39±0.48	5.21±0.42
50:2	9.00±0.18	8.37±0.61	7.66±0.65
50:1	7.90±1.31	7.78±0.33	11.12±0.30
48:3	7.13±0.35	7.30±1.20	4.00±0.47
48:1	6.82±0.15	7.65±0.25	9.68±1.24
48:2	6.28±0.32	6.34±0.23	5.24±0.07
60:1	5.06±0.63	4.25±0.71	7.11±1.19
52:2	4.89±0.09	4.37±0.33	4.46±0.13
52:3	4.58±1.24	3.68±0.30	2.10±0.23
52:1	4.10±0.88	3.32±0.97	7.23±0.46
58:1	3.98±0.54	3.86±0.79	6.61±1.48
44:1	3.75±0.06	4.18±0.52	3.12±0.28
42:1	2.72±0.28	3.69±0.13	2.06±0.25
46:1	2.58±0.13	3.17±0.57	2.14±0.39
60:2	1.39±0.16	1.25±0.20	1.52±0.08
58:2	1.02±0.18	0.91±0.08	0.88±0.08
54:1	0.97±0.35	0.65±0.50	1.78±0.84
54:2	0.90±0.07	0.76±0.00	0.75±0.17
53:3	0.84±0.05	0.84±0.11	0.43±0.06
46:2	0.81±0.13	1.09±0.11	0.53±0.03
44:0	0.66±0.16	0.79±0.23	1.05±0.06
56:1	0.66±0.01	0.71±0.12	0.84±0.08
50:0	0.64±0.24	0.74±0.20	0.87±0.09
52:0	0.64±0.09	0.79±0.08	0.91±0.03
58:0	0.63±0.22	0.66±0.21	0.90±0.14
53:2	0.61±0.03	0.50±0.07	0.52±0.07
54:3	0.60±0.14	0.46±0.11	0.33±0.08
51:1	0.58±0.17	0.50±0.13	0.79±0.28
53:1	0.56±0.08	0.50±0.11	0.73±0.14
44:2	0.55±0.01	0.88±0.21	0.37±0.04
47:1	0.52±0.01	0.86±0.18	0.43±0.08
51:2	0.52±0.00	0.60±0.05	0.50±0.08
51:3	0.51±0.03	0.59±0.03	0.29±0.04
48:6	0.51±0.05	1.04±0.14	0.64±0.17
42:0	0.46±0.09	0.62±0.09	0.70±0.09
55:2	0.45±0.10	0.26±0.02	0.29±0.03
48:0	0.44±0.09	0.63±0.31	0.71±0.03
55:3	0.43±0.04	0.38±0.02	0.25±0.04
54:0	0.35±0.07	0.54±0.27	0.60±0.22
59:1	0.33±0.15	0.39±0.10	0.73±0.18
46:0	0.31±0.03	0.41±0.41	0.59±0.14
55:1	0.30±0.21	0.40±0.12	0.50±0.05
44:5	0.30±0.22	0.18±0.16	0.11±0.06
60:0	0.22±0.04	0.28±0.08	0.54±0.18

47:2	0.21±0.00	0.37±0.07	0.16±0.01
56:0	0.21±0.10	0.13±0.07	0.05±0.02
44:4	0.21±0.18	0.05±0.05	0.11±0.11
57:3	0.17±0.04	0.08±0.04	0.07±0.07
53:4	0.17±0.04	0.15±0.03	0.11±0.03
49:3	0.17±0.05	0.29±0.11	0.10±0.08
58:6	0.16±0.04	0.13±0.02	0.07±0.06
46:3	0.15±0.01	0.23±0.04	0.09±0.04
56:2	0.14±0.02	0.10±0.01	0.10±0.08
57:6	0.13±0.04	0.14±0.02	0.10±0.04
57:1	0.12±0.11	0.09±0.07	0.01±0.01
57:2	0.10±0.06	0.10±0.06	0.08±0.07
56:6	0.09±0.01	0.07±0.07	0.02±0.02
49:0	0.09±0.09	0.01±0.01	0.01±0.01
45:1	0.08±0.05	0.08±0.04	0.04±0.01
47:3	0.08±0.04	0.14±0.04	0.05±0.02
51:4	0.07±0.01	0.06±0.05	0.04±0.03
49:2	0.06±0.03	0.03±0.03	0.05±0.05
57:0	0.06±0.04	0.06±0.06	0.06±0.06
43:0	0.06±0.04	0.05±0.04	0.06±0.06
53:0	0.07±0.05	0.03±0.03	0.00±0.00
43:1	0.06±0.04	0.09±0.07	0.02±0.02
52:4	0.06±0.02	0.07±0.04	0.04±0.03
50:5	0.06±0.04	0.04±0.04	0.01±0.01
41:1	0.05±0.04	0.00±0.00	0.02±0.02
55:0	0.05±0.04	0.03±0.03	0.00±0.00
55:4	0.05±0.03	0.00±0.00	0.01±0.01
47:5	0.05±0.03	0.03±0.01	0.00±0.00
56:4	0.03±0.03	0.01±0.01	0.00±0.00
58:5	0.03±0.01	0.01±0.01	0.02±0.02
50:4	0.03±0.02	0.03±0.03	0.03±0.03
48:4	0.03±0.02	0.01±0.01	0.04±0.04
40:0	0.03±0.02	0.02±0.02	0.01±0.01
60:4	0.03±0.01	0.05±0.03	0.05±0.04
40:1	0.03±0.02	0.01±0.01	0.01±0.01
60:12	0.02±0.02	0.01±0.00	0.01±0.00
46:5	0.02±0.02	0.01±0.01	0.03±0.00
58:3	0.02±0.00	0.01±0.01	0.01±0.01
60:3	0.02±0.01	0.01±0.01	0.01±0.00
49:4	0.02±0.01	0.05±0.02	0.03±0.03
46:4	0.02±0.01	0.01±0.00	0.01±0.01
44:3	0.02±0.00	0.02±0.02	0.02±0.02
56:3	0.02±0.01	0.01±0.01	0.01±0.01
47:4	0.02±0.01	0.01±0.01	0.01±0.01
45:0	0.02±0.01	0.12±0.11	0.04±0.04
54:6	0.01±0.01	0.03±0.02	0.03±0.03
57:4	0.01±0.01	0.08±0.08	0.05±0.05
41:5	0.01±0.00	0.02±0.02	0.01±0.01
59:2	0.00±0.00	0.01±0.01	0.01±0.00

59:0	0.00±0.00	0.00±0.00	0.00±0.00
40:2	0.00±0.00	0.00±0.00	0.00±0.00
41:4	0.00±0.00	0.00±0.00	0.00±0.00
41:3	0.00±0.00	0.00±0.00	0.00±0.00
41:2	0.00±0.00	0.00±0.00	0.00±0.00
41:0	0.00±0.00	0.00±0.00	0.00±0.00
42:5	0.00±0.00	0.00±0.00	0.00±0.00
42:4	0.00±0.00	0.00±0.00	0.00±0.00
42:3	0.00±0.00	0.01±0.01	0.00±0.00
42:2	0.00±0.00	0.17±0.15	0.07±0.07
43:2	0.00±0.00	0.00±0.00	0.00±0.00
45:5	0.00±0.00	0.00±0.00	0.00±0.00
45:4	0.00±0.00	0.00±0.00	0.00±0.00
45:3	0.00±0.00	0.00±0.00	0.00±0.00
45:2	0.00±0.00	0.00±0.00	0.00±0.00
47:0	0.00±0.00	0.00±0.00	0.00±0.00
48:5	0.00±0.00	0.00±0.00	0.00±0.00
49:5	0.00±0.00	0.01±0.00	0.02±0.01
49:1	0.00±0.00	0.07±0.07	0.06±0.06
51:5	0.00±0.00	0.01±0.01	0.03±0.03
51:0	0.00±0.00	0.00±0.00	0.00±0.00
52:5	0.00±0.00	0.00±0.00	0.00±0.00
53:5	0.00±0.00	0.00±0.00	0.03±0.03
54:5	0.00±0.00	0.00±0.00	0.03±0.03
54:4	0.00±0.00	0.00±0.00	0.00±0.00
55:6	0.00±0.00	0.00±0.00	0.00±0.00
55:5	0.00±0.00	0.00±0.00	0.00±0.00
56:5	0.00±0.00	0.00±0.00	0.03±0.03
57:5	0.00±0.00	0.01±0.01	0.01±0.01
58:4	0.00±0.00	0.02±0.02	0.00±0.00

Triacylglycerols (TAGs) were extracted from purified LDs, subjected to mass spectrometry, and identified. TAG molecular species and corresponding mol percentages for each are listed.

Supplemental Figure 1

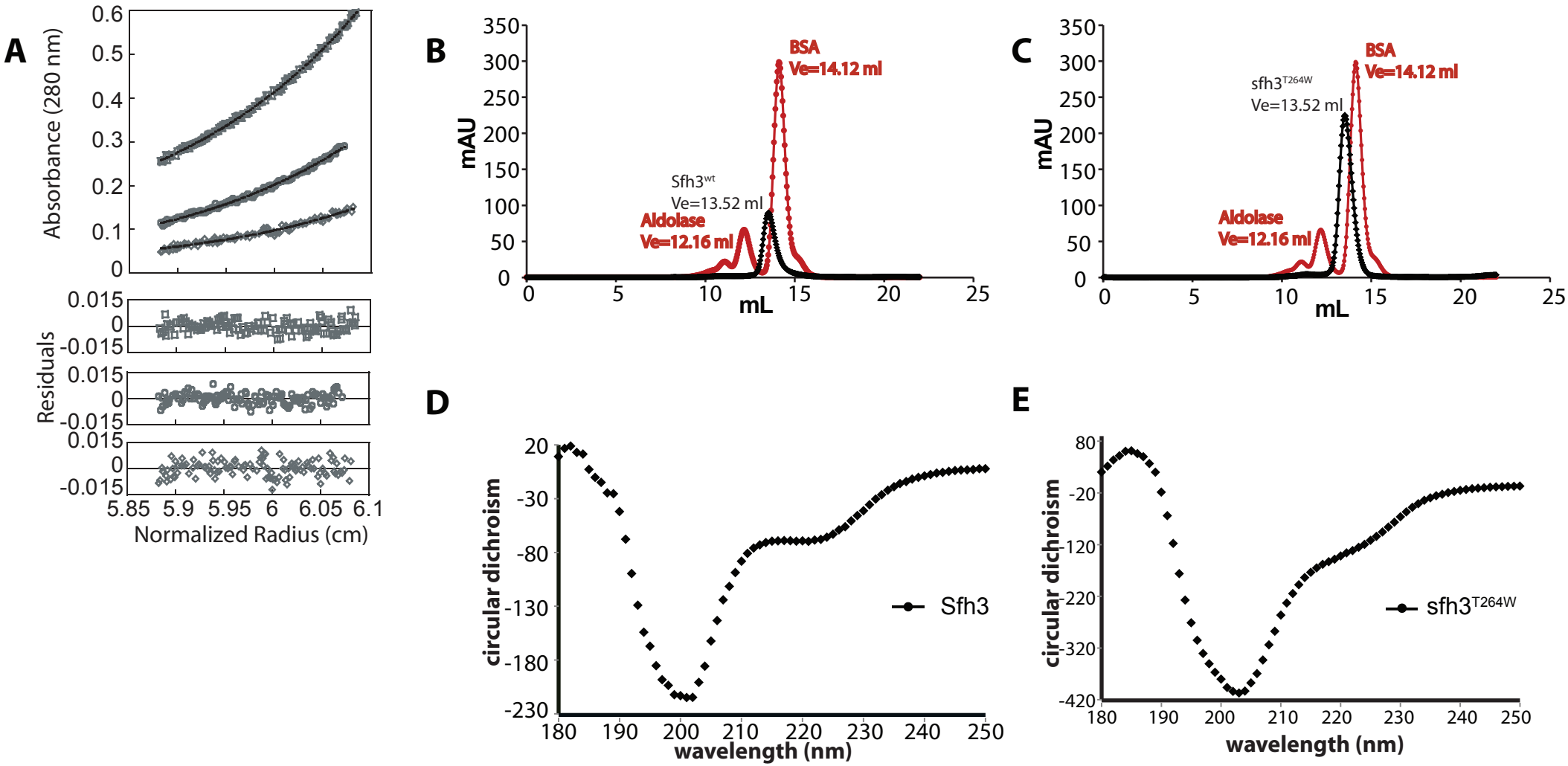

Supplemental Figure 3